ACS APPLIED MATERIALS & INTERFACES

www.acsami.org

Research Article

Mixed-Dimensional Van der Waals Heterostructure Photodetector

Jiaoyan Zhou, Mingzhang Xie, Huan Ji, Anyang Cui, Yan Ye, Kai Jiang, Liyan Shang, Jinzhong Zhang, Zhigao Hu,* and Junhao Chu

Cite This: *ACS Appl. Mater. Interfaces* 2020, 12, 18674−18682

Read Online

ACCESS | Metrics & More | Article Recommendations | Supporting Information

ABSTRACT: Van der Waals (vdW) heterostructures, integrated two-dimensional (2D) materials with various functional materials, provide a distinctive platform for next-generation optoelectronics with unique flexibility and high performance. However, exploring the vdW heterostructures combined with strongly correlated electronic materials is hitherto rare. Herein, a novel temperature-sensitive photodetector based on the GaSe/VO_2 mixed-dimensional vdW heterostructure is discovered. Compared with previous devices, our photodetector exhibits excellent enhanced performance, with an external quantum efficiency of up to 109.6% and the highest responsivity (358.1 mA·W^{-1}) under a 405 nm laser. Interestingly, we show that the heterostructure overcomes the limitation of a single material under the interaction between VO_2 and GaSe, where the photoresponse is highly sensitive to temperature and can be further vanished at the critical value. The metal−insulator transition of VO_2, which controls the peculiar band-structure evolution across the heterointerface, is demonstrated to manipulate the photoresponse variation. This study enables us to elucidate the method of manipulating 2D materials by strongly correlated electronic materials, paving the way for developing high-performance and special optoelectronic applications.

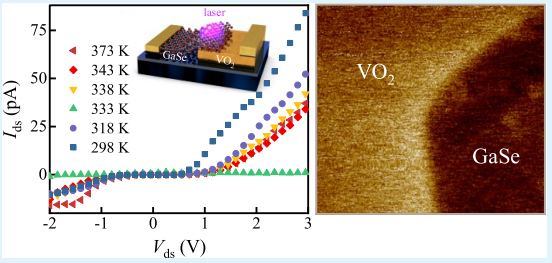

KEYWORDS: *vanadium dioxide, gallium selenide, mixed-dimensional van der Waals heterostructure, MIT-controlled photoresponse, band engineering*

1. INTRODUCTION

Van der Waals (vdW) heterostructures with two-dimensional (2D) atomically layered materials have been supposed to be the capable candidate for the photodetection in the broad range to replace and/or complement the conventional photodetectors.[1−4] Due to the weak vdW force, vdW heterostructure devices offer a unique bond-free integration approach for constructing the optoelectronic device. Compared with the devices assembled by the chemical bonds, this device not only gets rid of the limitations for lattice structures and required synthesis conditions in heteroepitaxy but also can be physically and freely assembled by diverse 2D materials according to the required functions.[5] Moreover, by designing the band structure in the vdW heterointerface, the device can display the high-performance or unique photoresponse phenomenon, which is prohibited in a single material.[1] Although vdW heterostructures have been widely explored in 2D devices, their applicability and prospects for photodetection combined with functional materials, especially strongly correlated electronic materials, have not been fully discovered. Strongly correlated electronic materials always exhibit the noteworthy optoelectronic properties and specific transitions between different electrical, magnetic, and lattice structure phases via external excitation, due to their internal electron−electron interaction.[6] These opulent phenomena are fascinating and offer possibilities to interact with 2D materials in vdW heterostructures for exploring highly responsive and special optoelectronic applications.

As one of the promising materials, vanadium dioxide (VO_2) is a typical n-type strongly correlated electronic material, which is of particular interest in the memristive element, optical switch, photodetection, and so on.[7−9] This is due to the fact that VO_2 undergoes an invertible metal−insulator transition (MIT) at a critical temperature (T_{MIT}),[10] with the variation in optical transmission and electrical resistivity by orders of magnitude. Meanwhile, the lattice structure is transformed between the rutile phase [VO_2(R), $P4_2/mnm$] and the monoclinic phase [VO_2(M), $P2_1/c$].[11,12] Moreover, due to the MIT, VO_2 can be used as an active layer to modulate the electrical and optical properties of other functional materials, such as the piezoelectric material,[13] functional oxide,[14] and photosensitive semiconductor.[15] As for 2D materials, exploring the vdW heterostructures integrated with the VO_2 is gradually starting. For example, Hou *et al.*[16] have investigated that the photoluminescence (PL) of MoS_2 can be modulated by the

Received: January 18, 2020
Accepted: March 25, 2020
Published: March 25, 2020

https://dx.doi.org/10.1021/acsami.0c01076
ACS Appl. Mater. Interfaces 2020, 12, 18674−18682

Table 1. Comparison of the Present Device Performance with Other GaSe-Based vdW Heterostructure Photodetectors Reported from the Literature

van der Waals heterostructure	wavelength (nm)	EQE (%)	R_{ph} (mA·W^{-1})	D^* (Jones)	LDR (dB)	on−off current ratio	ref
1 TL GaSe/$MoSe_2$	400−800	0.12	5.5				48
3 TL GaSe/MoS_2	300						34
8 TL GaSe/Si	532	23.6					21
multilayer GaSe/GaSb	637	50	115	2.2×10^{12}	77.51		49
3 TL GaSe/MoS_2	532		50	10^{10}	70	$>10^2$	42
15 TL GaSe/MoS_2	532		350		54		
15 TL GaSe/VO_2	405	109.6	358.1	2.14×10^{11}	81.2	433	this work[a]

[a]Note that the values of the present device are highly sensitive to the MIT of VO_2.

MIT of VO_2, where the PL intensity variation is related to the optical interference effect. Analogously, Lin *et al.*[17] have further explored the reversible optical modulation on monolayer MoS_2/VO_2 and WS_2/VO_2 heterostructures by switching the VO_2 phase between the insulator and the metal. Oliva *et al.*[18] have mainly probed the electronic characterization of the multilayer MoS_2/VO_2 heterostructure, which shows a tunable rectifier behavior. Nevertheless, there is a lack of study on the photodetection technology combining 2D materials with VO_2. Furthermore, due to the rich physical properties of VO_2, the mechanism of the interaction between the 2D materials and VO_2 in the vdW heterostructure is not clear, which plays a vital role in developing its potential optoelectronic applications.

Here, we report a comprehensive and significant study on a novel temperature-sensitive photodetector based on the high-quality gallium selenide (GaSe)/VO_2 vertical 2D/three-dimensional (3D) vdW heterostructures. GaSe is a p-type 2D semiconductor with the hexagonal crystal system, which is also in group III−VI semiconductor. It is a promising candidate for electronic and photonic devices due to its high photoresponsivity, a high field-effect on−off ratio, and diverse quantum confinement.[19,20] Furthermore, GaSe crystal displays a direct-to-indirect bandgap transformation from the bulk to the monolayer, along with a drop in the energy gap of only 25 meV, contrary to the common 2D materials.[21,22] However, due to difficulty in synthesis, there is a scarce study on GaSe and its vdW heterostructure. Our GaSe/VO_2 p−n junction with a type-II band structure exhibits the obvious rectifying characteristics, with an ultralow leakage current (down to 10^{-3} pA) and a high rectifying ratio (over 10^2). Excitingly, our vdW heterostructure device presents the excellent external quantum efficiency (EQE) (109.6%) under a 405 nm laser. The photoresponsivity is up to 358.1 mA·W^{-1}, with sensitive detectivity (2.14×10^{11} Jones) and the largest linear dynamic range (LDR) (81.2 dB). The repeatable and robust photoresponse, with the fast response speed, has been further demonstrated. These outstanding photodetection performances are well beyond the level of recently reported GaSe and vdW heterostructure devices, as shown in Table 1. Interestingly, the photoresponse of the GaSe/VO_2 heterostructure device is highly sensitive to temperature, which shows a nonlinear variation different from the reported black phosphorus,[23] graphene,[24] and InAs/InGaAs-[25]based photodetectors. Furthermore, the photocurrent can be quenched at the critical value and then re-emerged. It is actually controlled by the metal−insulator transition of VO_2, where temperature-dependent Kelvin probe force microscopy (KPFM) has been performed to characterize the peculiar band-structure evolution across the heterointerface during the MIT. This phenomenon is forbidden in a single material and is also the first discovery in the vdW heterostructure photodetector. This study paves the way for manipulating the optoelectronic properties of 2D materials by exploiting the fascinating physical characteristics of strongly correlated electronic materials in next-generation optoelectronic applications.

2. RESULTS AND DISCUSSION

2.1. Structural Analysis. The mixed-dimensional vdW heterostructure, in which the VO_2 film is combined with the GaSe flake, is prepared by pulsed laser deposition (PLD), mechanical exfoliation, and dry transfer in sequence. Figure 1A displays the typical cross-sectional transmission electron microscopy (TEM) image of the GaSe/VO_2 heterointerface prepared on the SiO_2/p^+-Si substrate, which shows a clear vertical stacked structure. The structural characterization and electrical properties of the VO_2 film are shown in Figures S1 and S2, which indicate that the VO_2 epitaxial film has a pure phase and good crystallization. The high-resolution TEM (HRTEM) of the VO_2 film is further performed in Figure 1B, whose inset shows the corresponding fast Fourier transform pattern. It also indicates good crystallization of the VO_2 film with a 0.24 nm lattice distance, which is consistent with the results of X-ray diffraction (XRD). The arithmetic-mean surface roughness of the VO_2 film measured by atomic force

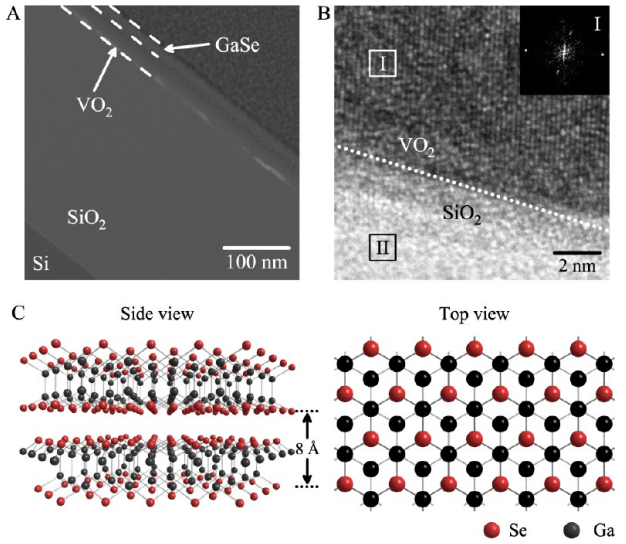

Figure 1. TEM characterization and atomic structure of the GaSe/VO_2 heterostructure. (A) Cross-sectional TEM image of the heterostructure. (B) HRTEM image of the VO_2 film with the corresponding FFT pattern in the inset. (C) Schematic diagram of the layered structure of GaSe, including the side and top views.

https://dx.doi.org/10.1021/acsami.0c01076
ACS Appl. Mater. Interfaces 2020, 12, 18674−18682

microscopy (AFM) is only 0.47 nm. The atomic flatness of the VO_2 film shows that it can be effectively integrated with 2D materials via the vdW force.[5,26] Furthermore, the VO_2 film presents a conspicuous metal−insulator transition around the MIT temperature (T_{MIT} ~ 338 K), which is slightly less than the theoretical temperature (340 K).[10] Meanwhile, Figure 1C represents the side and top views of the GaSe atomic structure. It exhibits a repeating tetra-layer (TL) structure with 8 Å thickness per TL, which is in the order of Se−Ga−Ga−Se. The exfoliated GaSe flakes belong to the ε-phase,[27,28] with an energy gap of 2.0 eV,[29,30] as shown in Figure S3. The detailed structural analysis of the GaSe/VO_2 heterostructure can be found in the Supporting Information.

2.2. Character of GaSe/VO_2 Heterostructure at Room Temperature. To investigate the potential application of the GaSe/VO_2 vdW heterostructure, the AFM and KPFM scannings are performed to characterize the corresponding architecture and electrical properties. Figure 2A and B show

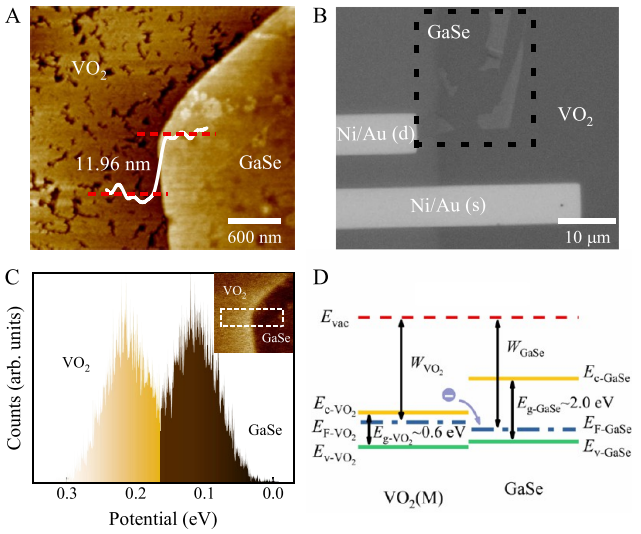

Figure 2. AFM and KPFM scannings of the GaSe/VO_2 heterostructure. (A) AFM topography and (B) optical images of the GaSe/VO_2 heterostructure. (C) Histogram obtained from the surface potential marked by a white-dashed rectangle in the inset, which is the KPFM surface potential image of the GaSe/VO_2 heterostructure at room temperature under dark conditions. (D) Band diagram of the GaSe/VO_2 p−n junction.

the AFM topography and optical images of a typical vertical GaSe/VO_2 mixed-dimensional heterostructure, respectively. The AFM height profile of the few-layer GaSe flake is 11.96 nm (~15 TL). As shown in Figure 2B, the GaSe flakes marked by the dotted box, which are split from the same exfoliated GaSe flake, have the same number of layers. The inset of Figure 2C displays the corresponding KPFM surface potential image of the GaSe/VO_2 heterostructure at room temperature under dark conditions, which is highly consistent with the AFM topography image. Figure 2C shows the surface potential of the white-dashed rectangle, which is summarized as a histogram. This illustrates that the Fermi level of the VO_2 film ($E_{F\text{-}VO_2}$) is higher than that of the GaSe flake ($E_{F\text{-}GaSe}$), with the Fermi level distinction (ΔE_F) of 0.14 eV. Hence, the work function of GaSe (W_{GaSe}) can be determined from the work function of VO_2 (W_{VO_2} ~ 5.15 eV)[31] at room temperature, which is approximately 5.29 eV and is in agreement with the previous studies.[32,33] Combining the schematic band diagrams of GaSe and VO_2,[32−36] the GaSe/VO_2 vdW heterostructure presents a type-II vertical p−n junction, as shown in Figure 2D. The electrons diffuse from VO_2 to GaSe to form a built-in potential drop with a depletion layer across the heterointerface. The characteristic of the p−n junction is further verified by the electrical measurement, as shown in Figure 3.

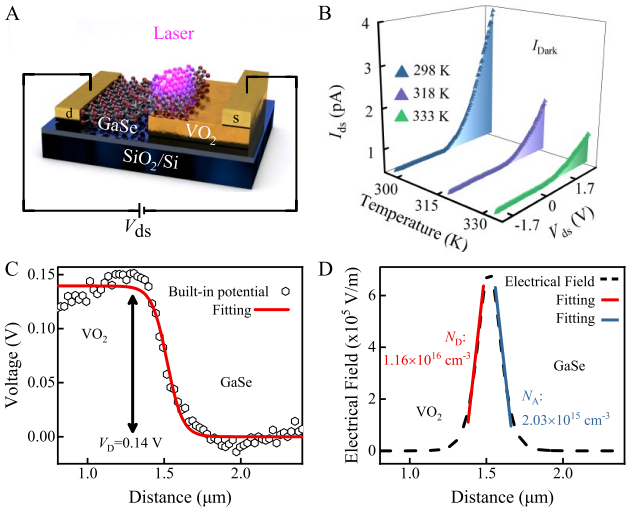

Figure 3. Electrical properties of the GaSe/VO_2 p−n junction. (A) Schematic illustration of the vertical GaSe/VO_2 vdW heterostructure device. The source and drain electrodes are deposited on the VO_2 film and the GaSe flake, respectively. (B) Temperature-dependent dark currents of the GaSe/VO_2 heterostructure. (C) Extracted built-in potential, and (D) built-in electric field across the GaSe/VO_2 heterointerface from the KPFM scanning.

Figure 3A shows the schematic of the GaSe/VO_2 heterostructure device fabricated on the SiO_2 (260 nm)/p^+-Si substrate. The patterned Ni/Au (5/38 nm) are deposited as the source and drain electrodes by thermal evaporation to complete the two-terminal device. The details can be found in Section 4. Around room temperature, the measured current−voltage (I_{ds}−V_{ds}) curve under dark conditions exhibits an anticipated rectification characteristic as the bias increases, which is attributed to the typical p−n junction formed at the *p*-GaSe/*n*-VO_2 heterointerface, as shown in Figure 3B. Due to the existence of the depletion layer and the energy barrier, the device exhibits an ultralow leakage current (down to 10^{-3} pA) and a high rectifying ratio (over 10^2) under the bias of ±2 V. Furthermore, the intrinsic characteristics of this p−n junction can be further determined. As shown in Figure 3C,D, the distributions of the built-in potential and the electric field can be obtained from the sigmoidal function fitting and Poisson equation, respectively.[37] Hence, the individual depletion widths in the VO_2 (d_n) and GaSe (d_p) can be calculated as an abrupt junction model,[38] which are approximately 0.04 and 0.23 μm, respectively. The carrier concentrations of the VO_2 film (N_D) and the GaSe flake (N_A) are estimated to be 1.16 × 10^{16} and 2.03 × 10^{15} cm^{-3}, respectively, which are highly consistent with the previously reported values.[39,40] More computational details can be found in the Supporting Information. Nevertheless, the temperature-dependent I_{ds}−V_{ds} curves of the device present an unusual variation, where I_{ds} decreases upon increasing the temperature below T_{MIT}. The rectifying ratio decreases from 229 to 40 under the bias of ±2

https://dx.doi.org/10.1021/acsami.0c01076
ACS Appl. Mater. Interfaces 2020, 12, 18674−18682

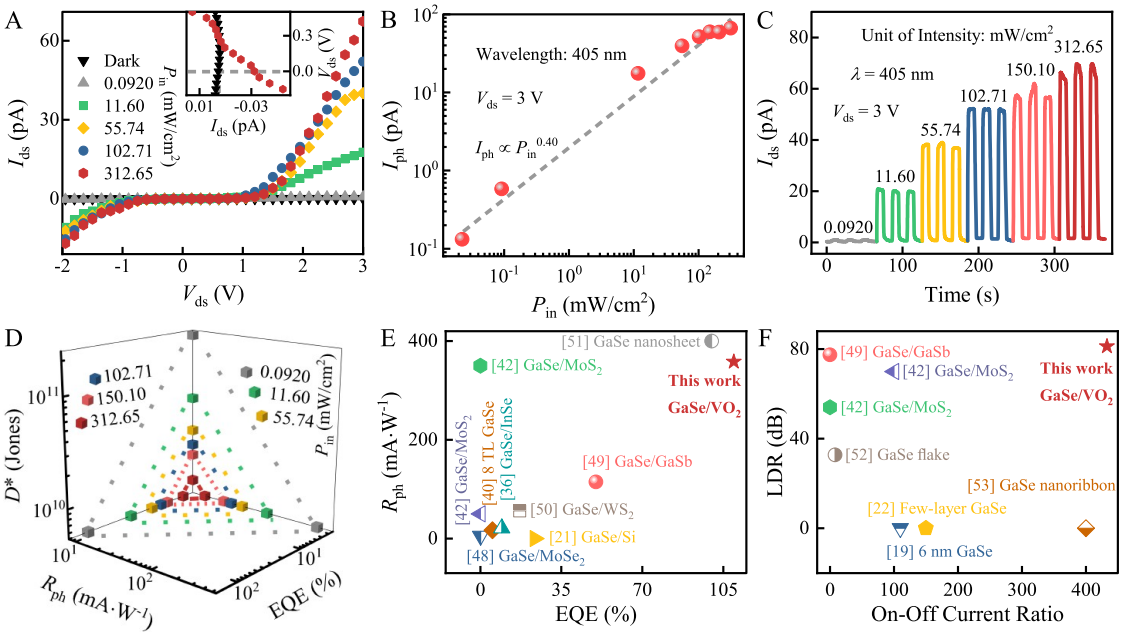

Figure 4. Optoelectronic properties of the GaSe/VO_2 photodetector. (A) I_{ds}−V_{ds} curves of the device at room temperature, which are measured under various irradiation intensities of a 405 nm laser and dark conditions. The inset shows the magnifying I_{ds}−V_{ds} curves around 0 V. (B) Dependence of the photocurrent on laser irradiation intensities (λ = 405 nm, V_{ds} = +3 V). (C) Incessant time-resolved photoresponse with various laser irradiation intensities (λ = 405 nm, V_{ds} = +3 V). (D) Corresponding EQE, responsivity (R_{ph}), and detectivity (D^*) values of the device as the functions of the irradiation intensity (λ = 405 nm, V_{ds} = +3 V). (E) EQE and R_{ph}, and (F) the on/off current ratio and LDR of our GaSe/VO_2 photodetector compared to recently reported photodetectors based on GaSe and other vdW heterostructures.

V. It is reverse with that described by the conventional p−n junction current equation $I = I_S(e^{qV/nk_BT} - 1)$. The abnormal variation trend of the rectifying current is attributed to the carrier concentration change of the GaSe/VO_2 p−n junction along with the temperature, which will be discussed in detail later. This indicates that the rectification characteristic of the device can be sensitively manipulated by the interaction between VO_2 with GaSe.

To explore the optoelectronic properties of the GaSe/VO_2 vdW heterostructure device, an excitation laser of 405 nm is employed. When the laser irradiates the heterostructure, the built-in electric field along the p−n junction facilitates the movements of the photogenerated electron−hole pairs to cause an obvious photovoltaic effect with an open-circuit voltage and short-circuit current, as shown in the inset of Figure 4A. Figure 4A further displays the I_{ds}−V_{ds} curves of the device under dark conditions and various irradiation intensities (P_{in} from 0.0920 to 321.65 mW·cm^{-2}). The photocurrent (I_{ph}) can be separated from $I_{ph} = I_{light} - I_{dark}$. A significant enhancement of I_{ph} at a fixed bias is observed as the laser irradiation intensity (P_{in}) increases. This occurs because the number of photogenerated carriers increases. The dependence of I_{ph} on P_{in} at a fixed bias can be expressed by a power law $I_{ph} \propto P_{in}^{\alpha}$,[41] as shown in Figure 4B. The α value is 0.40 at +3 V, which is less than 1. It is relevant to the trap states due to the defects from either the GaSe flake or the VO_2 film. By alternately tuning the on and off states of the laser, the time-resolved photoresponse cycle with increasing illumination intensity is observed, as shown in Figure 4C. The device shows a repeatable and robust response with high sensitivity to the 405 nm laser. The maximum on−off current ratio reaches up to 433. The dynamic response to the irradiation intensity can be fitted by $I(t) = I_0[1 - e^{-t/\tau}]$, where the response time τ comes up to 41 μs, which is much faster than the previous vdW devices.[21,34,42] The response time is mainly regulated by the lifetime of the photogenerated carriers, which is manipulated by the built-in electric field. Moreover, the excellent I_{ph} can also be conveniently obtained by increasing the bias voltage owing to the efficient separation of the photogenerated electron−hole pairs and the increase of the carrier velocity. According to Figure S4, the VO_2 film has almost no photoresponse with laser irradiation. The photogenerated carriers are mainly from the GaSe flake. Hence, the forward I_{ph} increases faster and is not saturated compared to the reverse I_{ph}, where the energy barrier of the GaSe/VO_2 p−n diode is reduced by the additional forward bias voltage.

To further illustrate the performance of the GaSe/VO_2 vdW heterostructure photodetector, the key parameters, such as responsivity (R_{ph}), external quantum efficiency (EQE), and detectivity (D^*), are explored, as shown in Figure 4D. The responsivity (R_{ph}) represents the efficiency of the detector in response to the incident light, which can be defined as follows

$$R_{ph} = \frac{I_{ph}}{P_{in}A} \tag{1}$$

where A is the effective area (A = 1.8 μm^2). Based on eq 1, the maximum value of R_{ph} can reach 358.1 mA·W^{-1} at V_{ds} = +3 V under an ultralow laser irradiation intensity of ∼0.0920 mW·cm^{-2}. The external quantum efficiency (EQE) indicates the number of photogenerated carriers per incident photon. Detectivity (D^*) indicates the sensitivity of the detector. EQE and D^* can be defined as the following eqs 2 and 3, respectively

$$\mathrm{EQE} = \frac{R_{ph}h\nu}{q} \tag{2}$$

https://dx.doi.org/10.1021/acsami.0c01076
ACS Appl. Mater. Interfaces 2020, 12, 18674−18682

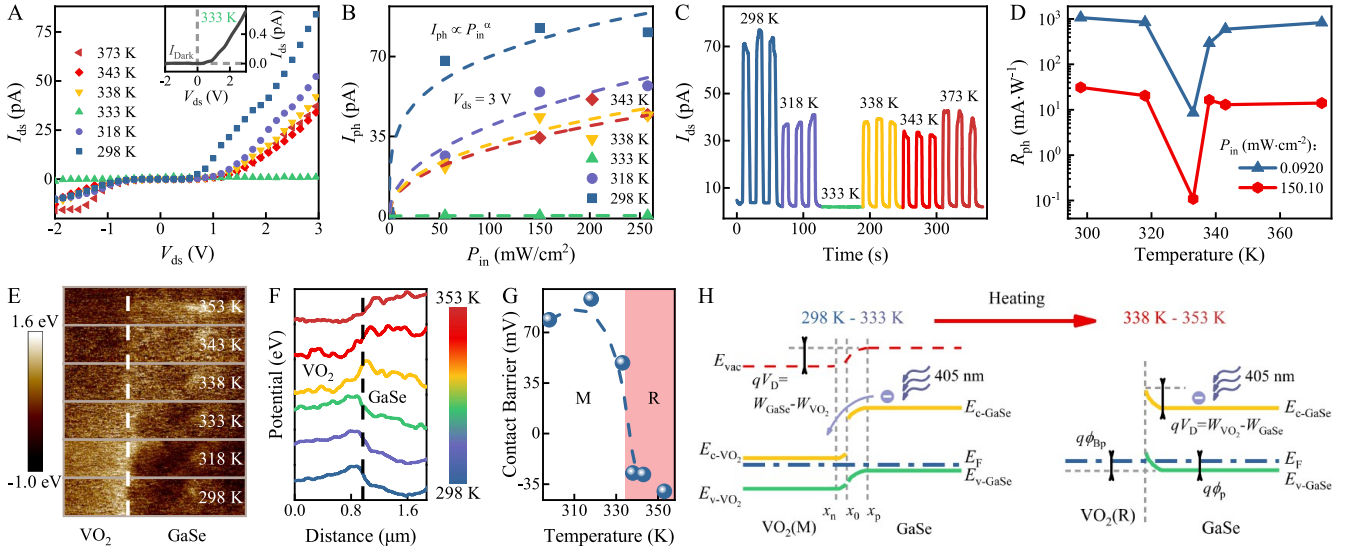

Figure 5. MIT-controlled photoresponse of the GaSe/VO_2 photodetector. (A) I_{ds}−V_{ds} curves across the heterostructure under 405 nm and 150.10 mW·cm^{-2} laser irradiation at various temperatures. The inset shows the dark current detected at 333 K. (B) Dependence of photocurrent on irradiation intensity at different temperatures (λ = 405 nm, V_{ds} = +3 V). (C) Incessant time-resolved photoresponse with various temperatures (λ = 405 nm, 150.10 mW·cm^{-2}, V_{ds} = +3 V). (D) Responsivity (R_{ph}) as the function of temperature at the representative laser irradiation intensities (λ = 405 nm, 0.0920, and 150.10 mW·cm^{-2}, V_{ds} = +3 V). (E) Temperature-dependent KPFM surface potential images of the GaSe/VO_2 heterostructure measured from 298 to 353 K. Note that the measured region is the same as the white-dashed rectangle. (F) Corresponding built-in potentials with variational temperature. (G) Temperature-dependent contact barrier. (H) Band-structure evolution of the GaSe/VO_2 p−n junction manipulated by the MIT.

$$D^* = \frac{R_{ph}A^{1/2}}{(2qI_{dark})^{1/2}} \tag{3}$$

where h is the Plank constant, ν is the frequency of light, q is the electron charge, and I_{dark} is the dark current, respectively. According to eqs 2 and 3, EQE and D^* can reach up to 109.6% and 2.14 × 10^{11} Jones at a bias of +3 V for the 405 nm laser, respectively. Moreover, the values of R_{ph}, EQE, and D^* are synchronously decreased by increasing the irradiation intensity, as shown in Figure 4D. It is attributed to the trap states in GaSe or VO_2. Under the weak light intensity, the photogenerated holes in GaSe can be captured by the trap states to prolong the lifetime of photogenerated electrons, which results in the high R_{ph}, EQE, and D^*. However, along with the increase in the light intensity, the existing trap states are reduced to further cause the saturation of the photodetection. The linear dynamic range (LDR) is another essential quality factor to evaluate the performance of the commercial complementary metal-oxide-semiconductor (CMOS) imaging sensor, which can be defined as LDR = 20 log(I_{light}/I_{dark}). The LDR value is required to exceed 60 dB for the imaging technique. The GaSe/VO_2 photodetector possesses the maximum value of LDR (~81.2 dB at V_{ds} = +3 V), which is also higher than the commercial InGaAs sensor (66 dB).[43] These above parameters are compared with many previously reported vdW photodetectors, as summarized in Table 1 and Figure 4E,F. It is quite clear that the GaSe/VO_2 vdW heterostructure is highly sensitive to the 405 nm laser and the photoresponse properties of our GaSe/VO_2 photodetector can rival or even surpass reported works, which are attributable to the high-quality GaSe/VO_2 p−n junction and the interaction between 2D materials and strongly correlated electronic materials.

2.3. MIT-Controlled GaSe/VO_2 Photodetector. The performance of the GaSe/VO_2 photodetector in this work is superior to the reported GaSe-based photodetectors. Due to the fascinating physical properties during the metal−insulator transition of the VO_2 film, we gain further insight into the manipulation behavior of the strongly correlated electronic material on our photodetector, as shown in Figure 5. Under the fixed irradiation intensity (150.10 mW·cm^{-2}), I_{ds} presents a nonmonotonic variation with temperature, which is suppressed gradually during the heating process until reaching the lowest value at 333 K. With further increase in the temperature, I_{ds} appears again and saturates above 338 K, as shown in Figure 5A. The inset shows that the dark current at 333 K still maintains the rectifying characteristic, which indicates that the GaSe/VO_2 heterostructure still worked as a p−n junction. Similarly, the power laws $I_{ph} \propto P_{in}^{\alpha}$ obtained at the fixed +3 V bias under different temperatures are plotted in Figure 5B. I_{ph} is vanished at 333 K concurrently at various irradiation intensities. Except for 333 K, I_{ph} upsurges immediately as the P_{in} rises, which still exhibits high sensitivity to the 405 nm laser. This peculiar optoelectronic property is also reflected in the time-resolved photoresponse cycle measured at 150.10 mW·cm^{-2} laser irradiation intensity and +3 V bias with various temperatures. The photoresponse is quenched when the temperature reaches 333 K. Then, the photoresponse is re-emerged as the temperature increases further, as shown in Figure 5C. Correspondingly, Figure 5D shows the same variations of R_{ph} along with the temperature under different laser irradiation intensities of 0.0920 and 150.10 mW·cm^{-2}. Under the irradiation of a weak laser and a strong laser, all of the values of R_{ph} approached a minimum at 333 K, which are further restored and saturated above 338 K. The above phenomena illustrate that the optoelectronic properties of the GaSe/VO_2 photodetector are highly sensitive to the temperature. Moreover, this nonlinear temperature-dependent photoresponse is absolutely dissimilar to the common 2D material-based[23,24] or heterostructure[25] photodetectors, whose photo-

https://dx.doi.org/10.1021/acsami.0c01076
ACS Appl. Mater. Interfaces 2020, 12, 18674−18682

response linearly varied with the temperature. However, the critical temperature, where the I_{ph} is vanished with quenched photoresponse, is highly close to the phase transition temperature of VO_2 from insulation to metal ($T_{MIT} \sim 338$ K). Along with the metal−insulator transition, the structure and electrical properties of the VO_2 exhibit the significant variations, which will further impact the electrical and optoelectronic properties of the GaSe/VO_2 vdW heterostructure. Hence, we deduce that the extraordinary photoresponse of the GaSe/VO_2 photodetector, which will be vanished at a critical temperature, is related to MIT of VO_2.

To shed light on the temperature-sensitive photoresponse mechanism of the device, the temperature-dependent KPFM is performed to demonstrate our inference. Figure 5E−G shows the variations of the surface potential and contact barrier along with the temperature. It is significant that the potential drop from VO_2 to GaSe is gradually reversed with the temperature. Synchronously, the contact barrier between VO_2 and GaSe is decreased to a negative value across MIT with a difference of 0.12 V. Obviously, it is related to the motion of $E_{F\text{-}VO_2}$ during the MIT. According to the previous study,[31] $E_{F\text{-}VO_2}$ is shifted to the low level with a ∼0.15 eV offset due to MIT, which is consistent with the measured value. Hence, a band engineering controlled by the MIT is displayed in Figure 5H, which exhibits the peculiar band-structure evolution of the GaSe/VO_2 heterointerface. Below T_{MIT} (∼338 K), $E_{F\text{-}VO_2}$ is still higher than $E_{F\text{-}GaSe}$, which indicates that the p−n junction is still in the type-II band alignment. However, the declined $E_{F\text{-}VO_2}$ reduces the degree of the donor ionization, which further drops the N_D and N_A for maintaining the electrical neutrality in the p−n junction,[44] as shown in Figure S5. Thus, the dark current and rectifying characteristics of the GaSe/VO_2 diode abnormally decrease as the temperature increases. Meanwhile, the declined $E_{F\text{-}VO_2}$ and ΔE_F also debilitate the built-in electric field, which further suppresses the separation of photogenerated electron−hole pairs. Hence, the photocurrent and photoresponse of the device decline with the increasing temperature.

Furthermore, there exists a critical temperature range (from 333 to 338 K), which is also around T_{MIT}. Within the critical temperature range, the $E_{F\text{-}VO_2}$ and $E_{F\text{-}GaSe}$ are equal to cause a flat-band phenomenon.[37] At the moment, the built-in electric field almost vanished and the photocurrent is hardly detected. In addition, the VO_2 film exhibits a mixed domain state around T_{MIT}, where the M and R phases coexist.[45,46] $E_{F\text{-}VO_2}$ of metallic VO_2(R) is transferred to the lower level than $E_{F\text{-}GaSe}$. Meanwhile, the contact between GaSe and metallic VO_2(R) is the Ohmic contact, whose heterointerface forms a p-type antibarrier layer, as shown in Figure 5H. The electrons easily move from the VO_2(R) to the GaSe due to the extremely low effective barrier height (ϕ_{Bp}). Hence, when the device is held around 333 K under a 405 nm laser irradiation, the photogenerated electrons are drifted from GaSe to VO_2(M) by the built-in electric field. Simultaneously, a similar amount of hot electrons are easily transported from VO_2(R) to GaSe, which results in a constant minority carrier concentration in the GaSe and the photocurrent is vanished. The photoresponse of the GaSe/VO_2 photodetector is also quenched around 333 K. Upon continuing to heat the heterostructure above T_{MIT} (∼338 K), the VO_2 film completely transformed into the metal state VO_2(R), which can be regarded as the electrode. The photocurrent of the GaSe/VO_2 photodetector, which re-emerged and reached the saturation above T_{MIT}, is only decided by the GaSe flake. Note that the metal−insulator transition manipulated photoresponse phenomenon is the first discovery in the vdW heterostructure photodetector. According to Figure S6, the variations of R_{ph}, EQE, and D^* both exhibit 2−3 orders of magnitude at the critical temperature. This indicates that the optoelectronic properties of the GaSe/VO_2 vdW heterostructure photodetector not only exhibits high performance but also is highly sensitive to the metal−insulator transition of VO_2. Meanwhile, the photocurrent and photoresponse can be further dynamically controlled for special optoelectronic applications by exerting external stimuli such as doping, temperature, electricity, and laser irradiation to manipulate the MIT behavior or alter the band structure.

3. CONCLUSIONS

In summary, we successfully fabricated a novel metal−insulator transition-controlled photodetector based on the GaSe/VO_2 vertical van der Waals heterostructure by PLD and dry transfer methods. The GaSe/VO_2 p−n junction shows a significant rectifying characteristic, with an ultralow leakage current (down to 10^{-3} pA) and a high rectifying ratio (over 10^2). Simultaneously, our heterostructure device exhibits the excellently enhanced photoresponse under a 405 nm laser, including the highest external quantum efficiency up to 109.6%, 358.1 mA·W^{-1} responsivity, and sensitive detectivity ($D^* \sim 2.14 \times 10^{11}$ Jones). The largest linear dynamic range (81.2 dB) and the high on−off current ratio (433) with the fast photoresponse speed have been further demonstrated. These outstanding performances outshine the recently reported GaSe and the corresponding vdW heterostructure photodetectors. Excitingly, when the VO_2 is transformed from the insulator-phase to the metal-phase with the increase in temperature, the photoresponse of the heterostructure device shows a unique nonlinear variation. The corresponding photocurrent is also highly sensitive to the MIT, which is further vanished around T_{MIT}. Meanwhile, the EQE, R_{ph}, and D^* exhibit changes of 2 or 3 orders of magnitude. The peculiar band-structure evolution of the heterointerface controlled by the MIT is characterized by the temperature-dependent KPFM to further interpret this photoresponse. These indicate that this heterostructure overcomes the limitation of a single material through the particular band engineering for high-performance and unique photoresponse characteristics, which is absolutely different from the conventional photodetector. This study illustrates the promise of the devising mixed-dimensional vdW heterostructure for the high-performance and special photodetector by utilizing the distinctive transitions of strongly correlated electronic material with the 2D materials.

4. EXPERIMENTAL SECTION

4.1. Material Synthesis. The pulsed laser deposition (PLD, TSST Customized) technique is employed to grow the 20 nm VO_2 epitaxial film on the p^+-Si substrate covered with the 260 nm SiO_2 (LIJINGKEJI Co., Ltd.).[47] To obtain the high-quality film, the substrate is cleaned in an ultrasonic bath with the pure acetone and ethanol, and flushed several times with deionized water. The VO_2 target is synthesized by VO_2 powders (purity 99.9%, Daheng Optics and Fine Mechanics Co., Ltd.). Before the deposition, the vacuum chamber is evacuated down to 7.09×10^{-5} mTorr. During the deposition process, the laser fluence incident upon the target surface is maintained at 2.12 J·cm^{-2} with a repetition rate of 10 Hz. Meanwhile, the oxygen partial pressure is maintained at 5 mTorr and

https://dx.doi.org/10.1021/acsami.0c01076
ACS Appl. Mater. Interfaces 2020, 12, 18674−18682

the substrate temperature is kept at room temperature. After deposition, the amorphous film is annealed at 450 °C under an argon atmosphere for 1 h to acquire the crystalline VO_2 films. Commercial bulk GaSe single crystals are purchased from HQ Graphene. The GaSe flakes with different thicknesses are prepared by the standard mechanical exfoliation method using Scotch tape (3M).

4.2. Device Fabrication. The GaSe flakes are exfoliated on the poly(dimethylsiloxane) stamp (PDMS, Gel-Pak) and immediately transferred onto the edge between the predeposited VO_2 film and the SiO_2 layer deterministically with the aligned system (E1-T, METATEST Co., Ltd.). Then, a layer of poly(methyl methacrylate) (PMMA 950K, Allresist) is spin-coated on the substrate with GaSe/VO_2 heterostructures. The spin coater (EZ4, Schwan Technology) is run for 10 s at 500 rpm and 60 s at 6000 rpm in sequence. After that, the substrate is baked at 150 °C for 3 min. Electron beam lithography (EBL, Raith PIONEER Two) is further carried out to delineate the electrodes. During development, after writing the standard pattern, the substrate is orderly soaked in the developer (AR 600-55, Allresist) for 60 s and the stopper (AR 600-60, Allresist) for 30 s. Then, Ni/Au (5/38 nm) layers are deposited to form the source and drain electrodes by the vacuum thermal evaporation (Type-300, KONG-MAILAI Co., Ltd.) at room temperature and a pressure of $\sim 10^{-3}$ mTorr. Finally, the substrate covered with PMMA and metal layers is soaked in the acetone for few minutes at room temperature to remove the extra metal. The patterned metal electrodes are exposed through the above lift-off process.

4.3. Characterization Methods. X-ray diffraction (XRD, Bruker D8 Advance diffractometer) with Cu Kα radiation (λ = 1.5418 Å) is employed to analyze the structural characteristics of the VO_2 films at room temperature. The thicknesses and the valence states are analyzed by scanning electron microscopy (SEM, Philips XL30FEG) and X-ray photoelectron spectroscopy (XPS, PerkinElmer RBD upgraded PHI-5000C ESCA system) with Mg Kα radiation ($h\nu$ = 1253.6 eV). The VO_2 films and GaSe/VO_2 heterostructures are further studied by the photoluminescence (PL) and temperature-dependent Raman spectra (Jobin-Yvon LabRAM HR Evolution spectrometer) with a 532 nm laser. The temperature is accurately controlled by a THMSE 600 heating/cooling stage (Linkam Scientific Instruments) in the range of 298−373 K. Atomic force microscopy (AFM, Bruker Dimension Icon) is performed to obtain the topographies of the VO_2 films and GaSe/VO_2 heterostructures, as well as the thicknesses of the exfoliated GaSe flakes. The cross-sections of the GaSe/VO_2 heterostructures are prepared by a focused ion beam (FIB, GAIA3 GMU model 2016) for transmission electron microscopy (TEM, JEOL 2100F) observation. The temperature-dependent current−voltage (I_{ds}−V_{ds}) and photoresponse properties are characterized by the Keithley 4200-SCS system from 298 to 373 K in the high vacuum environment ($\sim 10^{-4}$ mTorr). A 405 nm laser with varying irradiation intensities controlled by Thorlabs ITC4001 is focused on the VO_2 films and GaSe/VO_2 heterostructures with a 7.07 mm^2 spot. Moreover, the temperature-dependent Kelvin probe force microscopy (KPFM, Bruker Dimension Icon) under dark conditions is performed to quantitatively characterize the surface potential of the GaSe/VO_2 heterostructures. To ensure that the heterostructures reach the thermal equilibrium state during the measurement, the heating rate is accurately controlled at 5 K min^{-1} and temperature plateaus of 30 min. The temperature is varied from 298 to 353 K. Meanwhile, to avoid the oxidation, the detected samples are protected by the dry nitrogen atmosphere all the time.

■ ASSOCIATED CONTENT

Supporting Information

The Supporting Information is available free of charge at https://pubs.acs.org/doi/10.1021/acsami.0c01076.

Structural characterization of the VO_2 film (Section S1); XPS analysis of the VO_2 film (Section S2); structural analysis of the GaSe flake (Section S3); temperature-dependent electrical and optoelectronic characterization of the VO_2 film (Section S4); quantitative analysis of the KPFM scanning (Section S5); photoresponse of the GaSe/VO_2 photodetector varies with temperature (Section S6) (PDF)

■ AUTHOR INFORMATION

Corresponding Author

Zhigao Hu − *Technical Center for Multifunctional Magneto-Optical Spectroscopy (Shanghai), Engineering Research Center of Nanophotonics & Advanced Instrument (Ministry of Education), Department of Materials, School of Physics and Electronic Science, East China Normal University, Shanghai 200241, China; Collaborative Innovation Center of Extreme Optics, Shanxi University, Taiyuan, Shanxi 030006, China; Shanghai Institute of Intelligent Electronics & Systems, Fudan University, Shanghai 200433, China;* orcid.org/0000-0003-0575-2191; Phone: +86-21-54345150; Email: zghu@ee.ecnu.edu.cn; Fax: +86-21-54342933

Authors

Jiaoyan Zhou − *Technical Center for Multifunctional Magneto-Optical Spectroscopy (Shanghai), Engineering Research Center of Nanophotonics & Advanced Instrument (Ministry of Education), Department of Materials, School of Physics and Electronic Science, East China Normal University, Shanghai 200241, China*

Mingzhang Xie − *Technical Center for Multifunctional Magneto-Optical Spectroscopy (Shanghai), Engineering Research Center of Nanophotonics & Advanced Instrument (Ministry of Education), Department of Materials, School of Physics and Electronic Science, East China Normal University, Shanghai 200241, China*

Huan Ji − *Technical Center for Multifunctional Magneto-Optical Spectroscopy (Shanghai), Engineering Research Center of Nanophotonics & Advanced Instrument (Ministry of Education), Department of Materials, School of Physics and Electronic Science, East China Normal University, Shanghai 200241, China*

Anyang Cui − *Technical Center for Multifunctional Magneto-Optical Spectroscopy (Shanghai), Engineering Research Center of Nanophotonics & Advanced Instrument (Ministry of Education), Department of Materials, School of Physics and Electronic Science, East China Normal University, Shanghai 200241, China*

Yan Ye − *Technical Center for Multifunctional Magneto-Optical Spectroscopy (Shanghai), Engineering Research Center of Nanophotonics & Advanced Instrument (Ministry of Education), Department of Materials, School of Physics and Electronic Science, East China Normal University, Shanghai 200241, China*

Kai Jiang − *Technical Center for Multifunctional Magneto-Optical Spectroscopy (Shanghai), Engineering Research Center of Nanophotonics & Advanced Instrument (Ministry of Education), Department of Materials, School of Physics and Electronic Science, East China Normal University, Shanghai 200241, China*

Liyan Shang − *Technical Center for Multifunctional Magneto-Optical Spectroscopy (Shanghai), Engineering Research Center of Nanophotonics & Advanced Instrument (Ministry of Education), Department of Materials, School of Physics and Electronic Science, East China Normal University, Shanghai 200241, China*

https://dx.doi.org/10.1021/acsami.0c01076
ACS Appl. Mater. Interfaces 2020, 12, 18674−18682

Jinzhong Zhang − *Technical Center for Multifunctional Magneto-Optical Spectroscopy (Shanghai), Engineering Research Center of Nanophotonics & Advanced Instrument (Ministry of Education), Department of Materials, School of Physics and Electronic Science, East China Normal University, Shanghai 200241, China*

Junhao Chu − *Technical Center for Multifunctional Magneto-Optical Spectroscopy (Shanghai), Engineering Research Center of Nanophotonics & Advanced Instrument (Ministry of Education), Department of Materials, School of Physics and Electronic Science, East China Normal University, Shanghai 200241, China; Collaborative Innovation Center of Extreme Optics, Shanxi University, Taiyuan, Shanxi 030006, China; Shanghai Institute of Intelligent Electronics & Systems, Fudan University, Shanghai 200433, China*

Complete contact information is available at: https://pubs.acs.org/10.1021/acsami.0c01076

Author Contributions

This manuscript was written through contributions of all authors. All authors have given approval to the final version of the manuscript.

Notes

The authors declare no competing financial interest.

■ ACKNOWLEDGMENTS

This work was financially supported by the Natural Science Foundation of China (Grants Nos. 91833303, 61974043, and 61674057), the National Key Research and Development Program of China (Grants Nos. 2018YFB0406500, 2019YFB2203400, and 2017YFA0303403), Projects of Science and Technology Commission of Shanghai Municipality (Grant Nos. 18JC1412400, 18YF1407200, 18YF1407000, and 19511120100), and the Program for Professor of Special Appointment (Eastern Scholar) at Shanghai Institutions of Higher Learning.

■ REFERENCES

(1) Kim, K. S.; Ji, Y. J.; Kim, K. H.; Choi, S.; Kang, D.-H.; Heo, K.; Cho, S.; Yim, S.; Lee, S.; Park, J.-H.; Jung, Y. S.; Yeom, G. Y. Ultrasensitive MoS_2 Photodetector by Serial Nano-Bridge Multi-Heterojunction. *Nat. Commun.* **2019**, *10*, No. 4701.

(2) Massicotte, M.; Schmidt, P.; Vialla, F.; Schadler, K. G.; Reserbat-Plantey, A.; Watanabe, K.; Taniguchi, T.; Tielrooij, K. J.; Koppens, F. H. L. Picosecond Photoresponse in van der Waals Heterostructures. *Nat. Nanotechnol.* **2016**, *11*, 42−46.

(3) Xia, F. N.; Wang, H.; Xiao, D.; Dubey, M.; Ramasubramaniam, A. Two-dimensional Material Nanophotonics. *Nat. Photonics* **2014**, *8*, 899−907.

(4) Rivera, P.; Seyler, K. L.; Yu, H. Y.; Schaibley, J. R.; Yan, J. Q.; Mandrus, D. G.; Yao, W.; Xu, X. D. Valley-Polarized Exciton Dynamics in a 2D Semiconductor Heterostructure. *Science* **2016**, *351*, 688−691.

(5) Liu, Y.; Huang, Y.; Duan, X. F. Van der Waals Integration Before and Beyond Two-Dimensional Materials. *Nature* **2019**, *567*, 323−333.

(6) Morosan, E.; Natelson, D.; Nevidomskyy, A. H.; Si, Q. Strongly Correlated Materials. *Adv. Mater.* **2012**, *24*, 4896−4923.

(7) Kasırga, T. S.; Sun, D.; Park, J. H.; Coy, J. M.; Fei, Z. Y.; Xu, X. D.; Cobden, D. H. Photoresponse of a Strongly Correlated Material Determined by Scanning Photocurrent Microscopy. *Nat. Nanotechnol.* **2012**, *7*, 723−727.

(8) Chen, F. H.; Fan, L. L.; Chen, S.; Liao, G. M.; Chen, Y. L.; Wu, P.; Song, L.; Zou, C. W.; Wu, Z. Y. Control of the Metal-Insulator Transition in VO_2 Epitaxial Film by Modifying Carrier Density. *ACS Appl. Mater. Interfaces* **2015**, *7*, 6875−6881.

(9) Malarde, D.; Powell, M. J.; Quesada-Cabrera, R.; Wilson, R. L.; Carmalt, C. J.; Sankar, G.; Parkin, I. P.; Palgrave, R. G. Optimized Atmospheric-Pressure Chemical Vapor Deposition Thermochromic VO_2 Thin Films for Intelligent Window Applications. *ACS Omega* **2017**, *2*, 1040−1046.

(10) Morin, F. Oxides Which Show a Metal-to-Insulator Transition at the Neel Temperature. *Phys. Rev. Lett.* **1959**, *3*, 34−36.

(11) Morrison, V. R.; Chatelain, R. P.; Tiwari, K. L.; Hendaoui, A.; Bruhacs, A.; Chaker, M.; Siwick, B. J. A Photoinduced Metal-Like Phase of Monoclinic VO_2 Revealed by Ultrafast Electron Diffraction. *Science* **2014**, *346*, 445−448.

(12) Zhang, P.; Li, M. J.; Deng, Q. L.; Zhang, J. Z.; Wu, J. D.; Hu, Z. G.; Chu, J. H. Spectral Assignments in the Infrared Absorption Region and Anomalous Thermal Hysteresis in the Interband Electronic Transition of Vanadium Dioxide Films. *Phys. Chem. Chem. Phys.* **2016**, *18*, 6239−6246.

(13) Zhi, B. W.; Gao, G. Y.; Xu, H. R.; Chen, F.; Tan, X. L.; Chen, P. F.; Wang, L. F.; Wu, W. B. Electric-Field-Modulated Nonvolatile Resistance Switching in VO_2/PMN-PT(111) Heterostructures. *ACS Appl. Mater. Interfaces* **2014**, *6*, 4603−4608.

(14) Skuza, J. R.; Scott, D. W.; Mundle, R. M.; Pradhan, A. K. Electro-Thermal Control of Aluminum-Doped Zinc Oxide/Vanadium Dioxide Multilayered Thin Films for Smart-Device Applications. *Sci. Rep.* **2016**, *6*, No. 21040.

(15) Wang, Y. P.; Seewald, L.; Sun, Y.-Y.; Keblinski, P.; Sun, X.; Zhang, S. B.; Lu, T.-M.; Johnson, J. M.; Hwang, J.; Shi, J. Nonlinear Electron-Lattice Interactions in a Wurtzite Semiconductor Enabled Via Strongly Correlated Oxide. *Adv. Mater.* **2016**, *28*, 8975−8982.

(16) Hou, J.; Wang, X.; Fu, D. Y.; Ko, C.; Chen, Y. B.; Sun, Y. F.; Lee, S.; Wang, K. X.; Dong, K. C.; Sun, Y. H.; Tongay, S.; Jiao, L. Y.; Yao, J.; Liu, K.; Wu, J. Q. Modulating Photoluminescence of Monolayer Molybdenum Disulfide by Metal-Insulator Phase Transition in Active Substrates. *Small* **2016**, *12*, 3976−3984.

(17) Lin, Y.-C.; DeLello, K.; Zhang, H.-T.; Zhang, K.; Lin, Z.; Terrones, M.; Engel-Herbert, R.; Robinson, J. A. Photoluminescence of Monolayer Transition Metal Dichalcogenides Integrated with VO_2. *J. Phys.: Condens. Matter* **2016**, *28*, No. 504001.

(18) Oliva, N.; Casu, E. A.; Yan, C.; Krammer, A.; Rosca, T.; Magrez, A.; Stolichnov, I.; Schueler, A.; Martin, O. J. F.; Ionescu, A. M. Van der Waals MoS_2/VO_2 Heterostructure Junction with Tunable Rectifier Behavior and Efficient Photoresponse. *Sci. Rep.* **2017**, *7*, No. 14250.

(19) Zhou, Y.; Nie, Y. F.; Liu, Y. J.; Yan, K.; Hong, J. H.; Jin, C. H.; Zhou, Y.; Yin, J. B.; Liu, Z. F.; Peng, H. L. Epitaxy and Photoresponse of Two-Dimensional GaSe Crystals on Flexible Transparent Mica Sheets. *ACS Nano* **2014**, *8*, 1485−1490.

(20) Wei, X.; Yan, F. G.; Lv, Q. S.; Shen, C.; Wang, K. Y. Fast Gate-Tunable Photodetection in the Graphene Sandwiched WSe_2/GaSe Heterojunctions. *Nanoscale* **2017**, *9*, 8388−8392.

(21) Yuan, X.; Tang, L.; Liu, S. S.; Wang, P.; Chen, Z. G.; Zhang, C.; Liu, Y. W.; Wang, W. Y.; Zou, Y. C.; Liu, C.; Guo, N.; Zou, J.; Zhou, P.; Hu, W. D.; Xiu, F. X. Arrayed van der Waals Vertical Heterostructures Based on 2D GaSe Grown by Molecular Beam Epitaxy. *Nano Lett.* **2015**, *15*, 3571−3577.

(22) Yang, S. X.; Yue, Q.; Cai, H.; Wu, K. D.; Jiang, C. B.; Tongay, S. Highly Efficient Gas Molecule-Tunable Few-Layer GaSe Phototransistors. *J. Mater. Chem. C* **2016**, *4*, 248−253.

(23) Huang, M. Q.; Wang, M. L.; Chen, C.; Ma, Z. W.; Li, X. F.; Han, J. B.; Wu, Y. Q. Broadband Black-Phosphorus Photodetectors with High Responsivity. *Adv. Mater.* **2016**, *28*, 3481−3485.

(24) Zhang, Y. Z.; Liu, T.; Meng, B.; Li, X. H.; Liang, G. Z.; Hu, X. N.; Wang, Q. J. Broadband High Photoresponse from Pure Monolayer Graphene Photodetector. *Nat. Commun.* **2013**, *4*, No. 1811.

(25) Lu, X.; Vaillancourt, J.; Meisner, M. J. Temperature-Dependent Photoresponsivity and High-Temperature (190 K) Operation of a

Quantum Dot Infrared Photodetector. *Appl. Phys. Lett.* **2007**, *91*, No. 051115.
(26) Chow, C. M.; Yu, H. Y.; Jones, A. M.; Yan, J. Q.; Mandrus, D. G.; Taniguchi, T.; Watanabe, K. J.; Yao, W.; Xu, X. D. Unusual Exciton-Phonon Interactions at van der Waals Engineered Interfaces. *Nano Lett.* **2017**, *17*, 1194−1199.
(27) Wu, Y. C.; Zhang, D.; Lee, K.; Duesberg, G. S.; Syrlybekov, A.; Liu, X.; Abid, M.; Abid, M.; Liu, Y. Q.; Zhang, L. S.; Coileáin, C. Ó.; Xu, H. J.; Cho, J.; Choi, M.; Chun, B. S.; Wang, H. M.; Liu, H. J.; Wu, H. C. Quantum Confinement and Gas Sensing of Mechanically Exfoliated GaSe. *Adv. Mater. Technol.* **2017**, *2*, No. 1600197.
(28) Jie, W. J.; Chen, X.; Li, D.; Xie, L.; Hui, Y. Y.; Lau, S. P.; Cui, X. D.; Hao, J. H. Layer-Dependent Nonlinear Optical Properties and Stability of Non-Centrosymmetric Modification in Few-Layer GaSe Sheets. *Angew. Chem., Int. Ed.* **2015**, *54*, 1185−1189.
(29) Mahjouri-Samani, M.; Tian, M. K.; Wang, K.; Boulesbaa, A.; Rouleau, C. M.; Puretzky, A. A.; McGuire, M. A.; Srijanto, B. R.; Xiao, K.; Eres, G.; Duscher, G.; Geohegan, D. B. Digital Transfer Growth of Patterned 2D Metal Chalcogenides by Confined Nanoparticle Evaporation. *ACS Nano* **2014**, *8*, 11567−11575.
(30) Ceballos, F.; Bellus, M. Z.; Chiu, H. Y.; Zhao, H. Ultrafast Charge Separation and Indirect Exciton Formation in a MoS_2-$MoSe_2$ van der Waals Heterostructure. *ACS Nano* **2014**, *8*, 12717−12724.
(31) Ko, C.; Yang, Z.; Ramanathan, S. Work Function of Vanadium Dioxide Thin Films Across the Metal-Insulator Transition and the Role of Surface Nonstoichiometry. *ACS Appl. Mater. Interfaces* **2011**, *3*, 3396−3401.
(32) Kim, W.; Li, C. F.; Chaves, F. A.; Jiménez, D.; Rodriguez, R. D.; Susoma, J.; Fenner, M. A.; Lipsanen, H.; Riikonen, J. Tunable Graphene-GaSe Dual Heterojunction Device. *Adv. Mater.* **2016**, *28*, 1845−1852.
(33) Williams, R. H.; McEvoy, A. J. Surface Properties of the Gallium Monochalcogenides. *Phys. Status Solidi A* **1972**, *12*, 277.
(34) Zhou, N.; Wang, R. Y.; Zhou, X.; Song, H. Y.; Xiong, X.; Ding, Y.; Lv, J. T.; Gan, L.; Zhai, T. Y. P-GaSe/N-MoS_2 Vertical Heterostructures Synthesized by van der Waals Epitaxy for Photoresponse Modulation. *Small* **2018**, *14*, No. 1702731.
(35) Yang, Z.; Ko, C.; Ramanathan, S. Oxide Electronics Utilizing Ultrafast Metal-Insulator Transitions. *Annu. Rev. Mater. Res.* **2011**, *41*, 337−367.
(36) Yan, F.; Zhao, L.; Patanè, A.; Hu, P.; Wei, X.; Luo, W.; Zhang, D.; Lv, Q.; Feng, Q.; Shen, C.; Chang, K.; Eaves, L.; Wang, K. Fast, Multicolor Photodetection with Graphene-Contacted p-GaSe/n-InSe van der Waals Heterostructures. *Nanotechnology* **2017**, *28*, No. 27LT01.
(37) Jiang, T.; Wang, F.; Cui, A. Y.; Guo, S.; Jiang, K.; Shang, L. Y.; Hu, Z. G.; Chu, J. H. In Situ Exploration of the Thermodynamic Evolution Properties in the Type II Interface From WSe_2-WS_2 Lateral Heterojunction. *Nanotechnology* **2018**, *29*, No. 435703.
(38) Sze, S. M.; Ng, K. K. *Physics of Semiconductor Devices*; Wiley: New York, 1981; pp 77−133.
(39) Yang, Z.; Ko, C.; Balakrishnan, V.; Gopalakrishnan, G.; Ramanathan, S. Dielectric and Carrier Transport Properties of Vanadium Dioxide Thin Films Across the Phase Transition Utilizing Gated Capacitor Devices. *Phys. Rev. B* **2010**, *82*, No. 205101.
(40) Lei, S. D.; Ge, L. H.; Liu, Z.; Najmaei, S.; Shi, G.; You, G.; Lou, J.; Vajtai, R.; Ajayan, P. M. Synthesis and Photoresponse of Large GaSe Atomic Layers. *Nano Lett.* **2013**, *13*, 2777−2781.
(41) Wang, L.; Jie, J. S.; Shao, Z. B.; Zhang, Q.; Zhang, X. H.; Wang, Y. M.; Sun, Z.; Lee, S.-T. MoS_2/Si Heterojunction with Vertically Standing Layered Structure for Ultrafast, High-Detectivity, Self-Driven Visible-Near Infrared Photodetectors. *Adv. Funct. Mater.* **2015**, *25*, 2910−2919.
(42) Islam, A.; Lee, J.; Feng, P. X.-L. Atomic Layer GaSe/MoS_2 van der Waals Heterostructure Photodiodes with Low Noise and Large Dynamic Range. *ACS Photonics* **2018**, *5*, 2693−2700.
(43) Kim, C. O.; Kim, S.; Shin, D. H.; Kang, S. S.; Kim, J. M.; Jang, C. W.; Joo, S. S.; Lee, J. S.; Kim, J. H.; Choi, S.; Hwang, E. High Photoresponsivity in an All-Graphene *p-n* Vertical Junction Photodetector. *Nat. Commun.* **2014**, *5*, No. 3249.
(44) Doan, M. H.; Jin, Y.; Adhikari, S.; Lee, S.; Zhao, J.; Lim, S. C.; Lee, Y. H. Charge Transport in MoS_2/WSe_2 van der Waals Heterostructure with Tunable Inversion Layer. *ACS Nano* **2017**, *11*, 3832−3840.
(45) Holsteen, A.; Kim, I. S.; Lauhon, L. J. Extraordinary Dynamic Mechanical Response of Vanadium Dioxide Nanowires Around the Insulator to Metal Phase Transition. *Nano Lett.* **2014**, *14*, 1898−1902.
(46) Favaloro, T.; Suh, J.; Vermeersch, B.; Liu, K.; Gu, Y. J.; Chen, L. Q.; Wang, K. X.; Wu, J. Q.; Shakouri, A. Direct Observation of Nanoscale Peltier and Joule Effects at Metal-Insulator Domain Walls in Vanadium Dioxide Nanobeams. *Nano Lett.* **2014**, *14*, 2394−2400.
(47) Zhou, J. Y.; Xie, M. Z.; Cui, A. Y.; Zhou, B.; Jiang, K.; Shang, L. Y.; Hu, Z. G.; Chu, J. H. Manipulating Behaviors From Heavy Tungsten Doping on Interband Electronic Transition and Orbital Structure Variation of Vanadium Dioxide Films. *ACS Appl. Mater. Interfaces* **2018**, *10*, 30548−30557.
(48) Li, X. F.; Lin, M.-W.; Lin, J. H.; Huang, B.; Puretzky, A. A.; Ma, C.; Wang, K.; Zhou, W.; Pantelides, S. T.; Chi, M. F.; Kravchenko, I.; Fowlkes, J.; Rouleau, C. M.; Geohegan, D. B.; Xiao, K. Two-Dimensional GaSe/$MoSe_2$ Misfit Bilayer Heterojunctions by van der Waals Epitaxy. *Sci. Adv.* **2016**, *2*, No. e1501882.
(49) Wang, P.; Liu, S. S.; Luo, W. J.; Fang, H. H.; Gong, F.; Guo, N.; Chen, Z.-G.; Zou, J.; Huang, Y.; Zhou, X. H.; Wang, J. L.; Chen, X. S.; Lu, W.; Xiu, F. X.; Hu, W. D. Arrayed van der Waals Broadband Detectors for Dual-Band Detection. *Adv. Mater.* **2017**, *29*, No. 1604439.
(50) Lv, Q.; Yan, F.; Wei, X.; Wang, K. High-Performance, Self-Driven Photodetector Based on Graphene Sandwiched GaSe/WS_2 Heterojunction. *Adv. Optical Mater.* **2018**, *6*, No. 1700490.
(51) Mahjouri-Samani, M.; Gresback, R.; Tian, M.; Wang, K.; Puretzky, A. A.; Rouleau, C. M.; Eres, G.; Ivanov, I. N.; Xiao, K.; McGuire, M. A.; Duscher, G.; Geohegan, D. B. Pulsed Laser Deposition of Photoresponsive Two-Dimensional GaSe Nanosheet Networks. *Adv. Funct. Mater.* **2014**, *24*, 6365−6371.
(52) Hu, P.; Wen, Z.; Wang, L.; Tan, P.; Xiao, K. Synthesis of Few-Layer GaSe Nanosheets for High Performance Photodetectors. *ACS Nano* **2012**, *6*, 5988−5994.
(53) Xiong, X.; Zhang, Q.; Zhou, X.; Jin, B.; Lia, H.; Zhai, T. One-Step Synthesis of p-Type GaSe Nanoribbons and Their Excellent Performance in Photodetectors and Phototransistors. *J. Mater. Chem. C* **2016**, *4*, 7817−7823.

https://dx.doi.org/10.1021/acsami.0c01076
ACS Appl. Mater. Interfaces 2020, 12, 18674−18682